# Controller Design for an Induction Generator Driven by a Variable-Speed Wind Turbine

Woei-Luen Chen, *Member, IEEE*, and Yuan-Yih Hsu, *Senior Member, IEEE*

***Abstract*—This paper presents the modeling, controller design and a steady-state analysis algorithm for a wind-driven induction generator system. An output feedback linear quadratic controller is designed for the static synchronous compensator (STATCOM) and the variable blade pitch in a wind energy conversion system (WECS) in order to reach the voltage and mechanical power control under both grid-connection and islanding conditions. A two-reference-frame model is proposed to decouple the STATCOM real and reactive power control loops for the output feedback controller. To ensure zero steady-state voltage errors for the output feedback controller, the integrals of load bus voltage deviation and dc-capacitor voltage deviation are employed as the additional state variables. Pole-placement technique is used to determine a proper weighting matrix for the linear quadratic controller such that satisfactory damping characteristics can be achieved for the closed-loop system. Effects of various system disturbances on the dynamic performance have been simulated, and the results reveal that the proposed controller is effective in regulating the load voltage and stabilizing the generator rotating speed for the WECS either connected with or disconnected from the power grid. In addition, proper steady-state operating points for an isolated induction generator can be determined by the proposed steady-state analysis algorithm. Constant output frequency control using the derived steady-state characteristics of the isolated induction generator is then demonstrated in this paper.**

***Index Terms*—Induction generator (IG), static synchronous compensator (STATCOM), voltage regulation, wind energy conversion system (WECS), wind turbine.**

## NOMENCLATURE

*General*

| | |
|---|---|
| $e, \boldsymbol{E}$ | Inverter output voltage in instantaneous and vector notation. |
| $f_{\rm o}$ | Output frequency of the induction generator (IG) terminal voltage. |
| $\boldsymbol{I}$ | Identity matrix. |
| $i, \boldsymbol{I}$ | Current in instantaneous and vector notation. |
| $\boldsymbol{K}_s, \boldsymbol{K}_{\rm o}$ | State and output feedback gain matrices. |
| $P_m, P_g$ | Input mechanical power and output real power for the IG. |
| $r$ | Resistance. |
| $T_e, T_m$ | Electrical and mechanical torques. |
| $\boldsymbol{u}$ | Input vector. |
| $v, V, \boldsymbol{V}$ | Voltage in instantaneous, magnitude, and vector notation. |
| $V_w$ | Wind speed. |
| $X$ | Reactance. |
| $\boldsymbol{x}$ | State vector. |
| $\boldsymbol{y}$ | Output vector. |
| $\beta$ | Pitch angle of the wind turbine. |
| $\theta$ | Relative angular displacement for a specific vector, where $-\pi<\theta \leqq \pi$. |
| $\phi$ | Flux linkage. |
| $\omega$ | Angular frequency (angular speed). |
| $\boldsymbol{0}$ | Zero matrix. |

*Subscripts*

| | |
|---|---|
| $a$ | Vector or matrix for the augmented system. |
| $b$ | Base quantity. |
| $d, q$ | Quantities in $d$-axis and $q$-axis. |
| dc | dc link. |
| $f$ | Coupling transformer and filter for the STATCOM. |
| FC | Fixed shunt capacitor. |
| $L$ | Load. |
| $s, r$ | Stator and rotor. |
| $T$ | Wind turbine. |
| TL | Transmission line. |
| $\infty$ | Grid (infinite bus). |
| 0 | Initial operating point. |

*Superscripts*

| | |
|---|---|
| $T$ | Matrix transpose operator. |
| $*$ | Reference value. |

Manuscript received May 25, 2005; revised January 14, 2006. This work was supported by the National Science Council Taiwan, R.O.C., China under Contract NSC-93-2213-E-002-011. Paper no. TEC-00173-2005.

W.-L. Chen is with the Department of Electrical Engineering, National Taiwan University, and also with the Department of Electronic Engineering, Hwa Hsia Institute of Technology, Taipei 235, Taiwan, R.O.C. (e-mail: hr47131@cc.hwh.edu.tw).

Y.-Y. Hsu is with the Department of Electrical Engineering, National Taiwan University, Taipei 106, Taiwan, R.O.C. (e-mail: yyhsu@cc.ee.ntu.edu.tw).

Digital Object Identifier 10.1109/TEC.2006.875478

## I. INTRODUCTION

INDUCTION generators are being increasingly utilized in a wind energy conversion system (WECS) since they are relatively inexpensive, rigid, and require low maintenance. However, the impact of ever-changing wind speed on power quality, coupled with the need of excitation current for induction generator (IG), make the mechanical power control and voltage regulation indispensable to the wind-driven induction generator system. By far, the most effective way of controlling the mechanical power captured by the wind turbine is to adjust the rotor blade pitch angle. Blade pitch is analogous to the throttle valve in conventional steam turbines, except that the speed of control is much faster than the governor control in a steam turbine [1], [2]. It can be employed to regulate mechanical power input and real power output of the WECS. However, the reactive power required by the IG can be provided by a shunt capacitor bank, but it may cause excessive overvoltage during disconnection. Moreover, the amount of capacitance required for excitation varies

with the generator speed [3]. Thus, if a fixed shunt capacitor is connected across the terminals of the IG, the terminal voltage will vary with generator speed. To achieve continuous voltage regulation under varying system conditions, static synchronous compensators (STATCOMs), have been employed in the literatures [4]–[8]. The basic principle of a STATCOM installed in a power system is to generate a controllable ac voltage behind a coupling transformer and a filter by a voltage-sourced inverter (VSI) connected to a dc capacitor. The output voltage of the VSI can be controlled to be greater than the line voltage in order to provide reactive power to the wind-driven IG.

An application of the linearized multivariable output feedback technique to the design of a voltage and mechanical power regulator for a wind turbine-induction generator around a specific operating point was given in [1], [9]. Nevertheless, for the WECS, it is impractical and uneconomical to fix the generator output power (or rotor speed) at a specific operating point since the wind speed changes all the time. Besides, the controller design based on the constant output power (or rotor speed) considerations under grid-connection condition would fail in islanding operation.

In this paper, an output feedback controller is designed to regulate system voltage and mechanical power under both grid-connection and islanding conditions. The major features of the proposed output feedback controller are summarized as follows.

1) A systematic approach based on pole placement technique has been applied to determine proper weighting matrix for the linear quadratic controller such that the eigenvalues for the closed-loop system can be shifted to desirable locations. As a result, satisfactory transient excursion suppression in system voltages and generator speed can be reached by the controller when the WECS is subjected to major disturbances.
2) The integrals of load bus voltage deviation and dc-capacitor voltage deviation are employed as additional state variables to eliminate the steady-state voltage errors for the output feedback controller.
3) A control scheme with two reference frames is proposed to reach the decoupled control for the STATCOM real and reactive power control loops in case of voltage fluctuations, no matter what kind of disturbances may take place.
4) A simple algorithm is developed to determine proper steady-state operating points for an isolated IG. Using the relationship between the generator speed and the output power at various frequencies, a proportional-integral controller is proposed to achieve constant frequency control for an isolated IG with sufficient mechanical power.

## II. System Models

Fig. 1 depicts the one-line diagram of an induction generator driven by a variable-speed wind turbine and connected to a grid through a transmission line. An output feedback controller is utilized to control the wind turbine mechanical power and the system reactive power through the variable blade pitch and the STATCOM, respectively. The reactive power required by the IG in steady-state operating condition is supplied by a fixed shunt capacitor bank, as shown in Fig. 1. To maintain constant load bus voltage $(V_L)$ under disturbance conditions, a STATCOM, which is capable of adjusting its output voltage and reactive power output based on system requirements, is employed. The STATCOM is connected to the load bus through a coupling transformer and a filter. Note that a constant impedance load is assumed in Fig. 1.

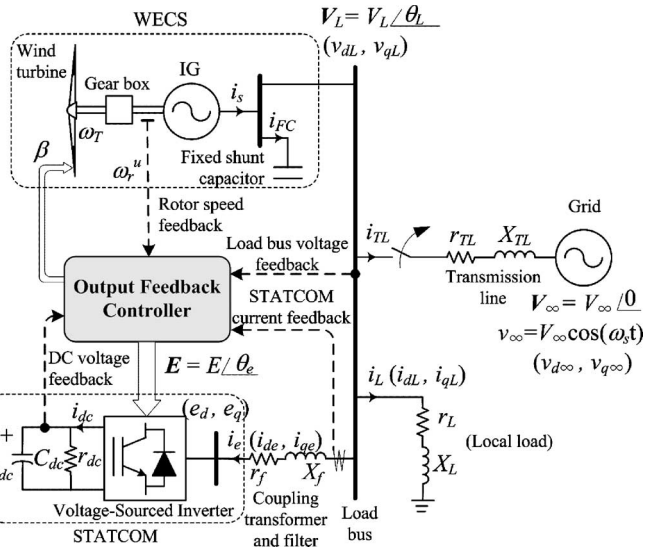


Fig. 1. System configuration.

### A. Induction Generator Model

The per unit flux-linkages for the stator and rotor circuits of the induction generator described in $d$- and $q$-axes are as follows [9], [10]:

$$\dot{\phi}_{ds} = \omega_b(v_{dL} + r_s i_{ds}) + \omega_s \phi_{qs} \tag{1}$$

$$\dot{\phi}_{qs} = \omega_b(v_{qL} + r_s i_{qs}) - \omega_s \phi_{ds} \tag{2}$$

$$\dot{\phi}_{dr} = \omega_b(v_{dr} - r_r i_{dr}) + (\omega_s - \omega_r)\phi_{qr} \tag{3}$$

$$\dot{\phi}_{qr} = \omega_b(v_{qr} - r_r i_{qr}) - (\omega_s - \omega_r)\phi_{dr} \tag{4}$$

where a synchronous reference frame rotating at the electrical angular speed corresponding to the fundamental frequency of the grid voltage, herein denoted as $\omega_s$, is adopted.

The electromechanical torque in per unit can be written in terms of stator flux linkages and currents as

$$T_e = \phi_{ds} i_{qs} - \phi_{qs} i_{ds}. \tag{5}$$

The per unit rotor acceleration is given by

$$\dot{\omega}_r^u = \frac{1}{2H_T}\left(T_m - T_e - D_T \omega_r^u\right) \tag{6}$$

where $T_m$ is the per unit mechanical torque of the wind turbine, and $H_T$ and $D_T$ are the equivalent inertia constant and the equivalent damping constant of the wind turbine-induction generator system, respectively.

### B. Wind Turbine Model

The mechanical power output of a wind turbine can be written as [2]

$$P_m = \frac{1}{2}\rho A C_p V_w^3 \tag{7}$$

where $\rho$ is the air mass density, $V_w$ is the wind speed, $A$ is the rotor swept area, and $C_p$ is a power coefficient representing the fraction of power extracted from the aerodynamic power in the wind by a practical wind turbine.

The power coefficient $C_p$ varies with the wind speed, the rotational speed of the turbine, and the turbine blade parameters. The MOD-2 wind turbine model [11], [12] with the following closed-form approximate relationship for $C_p$ is used:

$$C_p = \frac{1}{2}\left(\frac{R}{\gamma} - 0.022\beta^2 - 5.6\right) e^{-\frac{0.17R}{\gamma}}. \tag{8}$$

The tip speed ratio $\gamma$ is defined as

$$\gamma = \frac{\omega_T R}{V_w} \tag{9}$$

where $\omega_T$ is the rotating speed of the wind turbine as shown in Fig. 1.

It is observed from (7)–(9) that the mechanical power output of a wind turbine is related to the turbine speed $\omega_T$, wind speed $V_w$, and the pitch angle $\beta$. An increase in the pitch angle $\beta$, which results in a decrease in the power coefficient $C_p$, is efficient to control the mechanical power of the wind turbine when $P_m$ continues to increase with increasing wind speed.

In this work, the initial pitch angle $(\beta_0)$ is chosen to be 13.46° such that the wind turbine delivers a mechanical power of 0.81 per unit (p.u.) for a 30 miles/h (mph) wind at hub height. A hydraulic pitch angle actuator with a rate limit of ±10°/s and a transport delay of 50 ms [11], [12] is used in this paper.

### C. STATCOM Model

For a balanced three-phase system, the STATCOM model can be described in per unit using the variables in $d$- and $q$-axes synchronous reference frame as [4]

$$\dot{i}_{de} = -\frac{\omega_b r_f}{X_f} i_{de} + \omega_s i_{qe} + \frac{\omega_b}{X_f}(v_{dL} - e_d) \tag{10}$$

$$\dot{i}_{qe} = -\frac{\omega_b r_f}{X_f} i_{qe} - \omega_s i_{de} + \frac{\omega_b}{X_f}(v_{qL} - e_q). \tag{11}$$

In Fig. 1, the instantaneous powers at the ac and dc sides of the voltage-sourced inverter are equal, giving the following power balance equation:

$$v_{\rm dc} i_{\rm dc} = e_d i_{de} + e_q i_{qe}. \tag{12}$$

The per unit dc-side circuit equation is

$$\dot{v}_{\rm dc} = \frac{1}{C_{\rm dc}}\left(i_{\rm dc} - \frac{v_{\rm dc}}{r_{\rm dc}}\right) \tag{13}$$

where $r_{\rm dc}$ is used to represent the inverter switching loss.

The per unit equations of the fixed shunt capacitor, transmission line, and local load models are given in the Appendix.

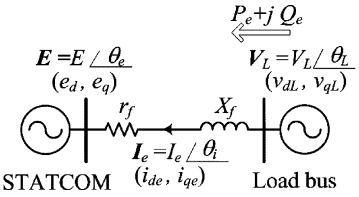


Fig. 2. Power flow between STATCOM and the load bus.

## III. Derivation of the Augmented State Equations

In order todetermine proper control signal for the STATCOM through a systematic design approach, the dynamic system equations as given in Section II are linearized around a nominal operating point in the form as

$$\dot{\Delta}\boldsymbol{x} = \boldsymbol{A}\cdot\Delta\boldsymbol{x} + \boldsymbol{B}\cdot\Delta\boldsymbol{u}$$
$$\Delta\boldsymbol{y} = C\cdot\Delta\boldsymbol{x} \tag{14a}$$

where

$$\Delta\boldsymbol{x} = [\Delta v_{dL} \quad \Delta v_{qL} \quad \Delta i_{dL} \quad \Delta i_{qL} \quad \Delta\omega_r^u \quad \Delta v_{\rm dc} \quad \Delta\phi_{qr} \quad \Delta\phi_{dr} \quad \Delta\phi_{ds} \quad \Delta\phi_{qs} \quad \Delta i_{d\rm TL} \quad \Delta i_{q\rm TL} \quad \Delta i_{de} \quad \Delta i_{qe}]^T \tag{14b}$$

is the state vector. It remains now to define the control action $\Delta\boldsymbol{u}$ and the output vector $\Delta\boldsymbol{y}$ based on the two-reference-frame transformation described below.

### A. Decoupled Control Using the Two-Reference-Frame Transformation

The purpose of the STATCOM controller is to make use of the real power and reactive power exchange between the STATCOM and the ac system to achieve good regulation of dc-capacitor voltage and the load bus voltage. In other words, STATCOM control is closely linked to the power flow at the STATCOM terminal, as shown in Fig. 2. It is well known [4], [5] that the instantaneous real and reactive power, through a coupling path to the STATCOM, at the load bus can be represented as follows:

$$P_e = v_{dL} i_{de} + v_{qL} i_{qe} \tag{15a}$$

$$Q_e = v_{qL} i_{de} - v_{dL} i_{qe}. \tag{15b}$$

Note that the $d$–$q$ quantities of the STATCOM current ($i_{de}$ and $i_{qe}$), STATCOM voltage ($e_d$ and $e_q$), and load bus voltage ($v_{dL}$ and $v_{qL}$) in (10), (11), and (15) are derived by choosing the vector for grid bus voltage $\boldsymbol{V}_\infty$ as the $d$-axis. To decouple the STATCOM real and reactive power control loops, a new reference frame which uses the vector for load bus voltage $\boldsymbol{V}_L$ as the new $d$-axis (denoted as $d'$-axis) is defined in Fig. 3 [4]. Note that the angles $\theta_e$, $\theta_L$, and $\theta_i$ in Fig. 3 are the phase angles for the voltages $\boldsymbol{E}$, $\boldsymbol{V}_L$, and STATCOM current $\boldsymbol{I}_e$, with respect to the original $d$-axis, respectively. On the other hand, the angles $\theta_e'$ and $\theta_i'$ in Fig. 3 are the phase angles for the voltage $\boldsymbol{E}$ and STATCOM current $\boldsymbol{I}_e$ with respect to the new $d'$-axis, respectively. As shown in Fig. 4, the voltages $e_d'$ and $e_q'$ and currents $i_{de}'$ and $i_{qe}'$ in the new reference frame are related to the

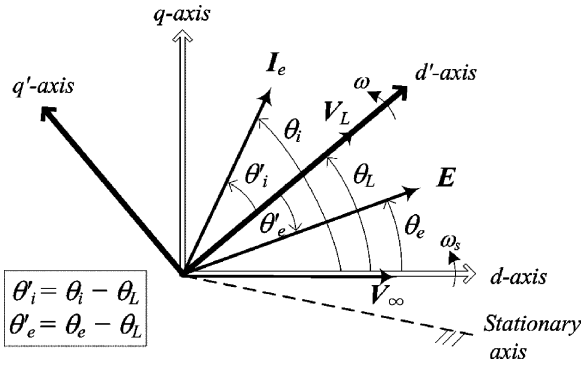


Fig. 3. Transformation between the two reference frames illustrated by trigonometric relationships.

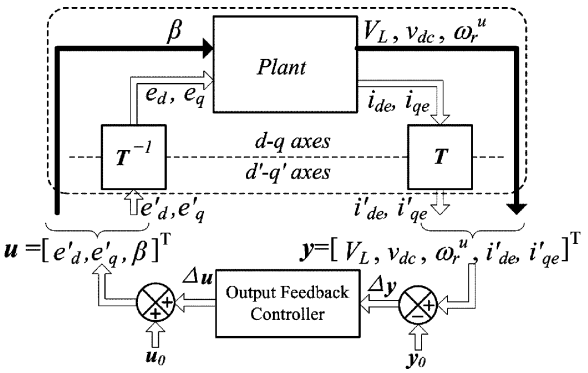


Fig. 4. Block diagram of the proposed output feedback controller.

voltages $e_d$ and $e_q$ and currents $i_d$ and $i_q$ in the original reference frame through the transformation matrix $\boldsymbol{T}$ as described below.

$$\begin{bmatrix} i'_{de} \\ i'_{qe} \end{bmatrix} = \mathbf{T} \begin{bmatrix} i_{de} \\ i_{qe} \end{bmatrix} \quad \text{and} \quad \begin{bmatrix} e'_d \\ e'_q \end{bmatrix} = \mathbf{T} \begin{bmatrix} e_d \\ e_q \end{bmatrix} \tag{16}$$

where

$$\boldsymbol{T} = \begin{bmatrix} \cos\theta_L & \sin\theta_L \\ -\sin\theta_L & \cos\theta_L \end{bmatrix}.$$

Using the d–q quantities $v'_{dL}$ (which is equal to $V_L$), $i'_{de}$, and $i'_{qe}$ in the new reference frame, the real and reactive powers in (15) can be written as

$$P_e = v'_{dL} i'_{de} \tag{17a}$$

$$Q_e = -v'_{dL} i'_{qe}. \tag{17b}$$

As (17) shows, the $d'$-axis current component $i'_{de}$ accounts for the instantaneous real power and the q′-axis current component $i'_{qe}$ is the instantaneous reactive current. Thus, STATCOM control design is simplified to a great extent with this new reference frame since the load bus voltage regulation is achievable through the control of the reactive power $Q_e$ which only related to the q′-axis current $i'_{qe}$.

Evidently, the transformation matrix $\boldsymbol{T}$ as described in (16) and its inverse are needed to transform certain system variables from the synchronous reference frame to the other in order to decouple STATCOM real and reactive power control loops for the proposed controller, as shown in Fig. 4. Thus, the control inputs for the state equations in (14a) are

$$\Delta \boldsymbol{u} = [\Delta e'_d \quad \Delta e'_q \quad \Delta\beta]^T \tag{18}$$

and the output vector is as follows:

$$\begin{aligned} \Delta \boldsymbol{y} &= \begin{bmatrix} \Delta V_L & \Delta v_{\rm dc} & \Delta\omega_r^u & \Delta i'_{de} & \Delta i'_{qe} \end{bmatrix}^T \\ &= \boldsymbol{C} \Delta \boldsymbol{x} \end{aligned} \tag{19}$$

where the output matrix $\boldsymbol{C}$ is given by

$$\boldsymbol{C} = \begin{bmatrix} \boldsymbol{C}_1^T & \boldsymbol{C}_2^T & \boldsymbol{C}_3^T & \boldsymbol{C}_4^T & \boldsymbol{C}_5^T \end{bmatrix}^T$$

and the submatrices $\boldsymbol{C}_1$, $\boldsymbol{C}_2$, $\boldsymbol{C}_3$, $\boldsymbol{C}_4$, and $\boldsymbol{C}_5$ are defined as $\Delta V_L = \boldsymbol{C}_1 \Delta \boldsymbol{x}$, $\Delta v_{\rm dc} = \boldsymbol{C}_2 \Delta \boldsymbol{x}$, $\Delta\omega_r^u = \boldsymbol{C}_3 \Delta \boldsymbol{x}$, $\Delta i'_{de} = \boldsymbol{C}_4 \Delta \boldsymbol{x}$, and $\Delta i'_{qe} = \boldsymbol{C}_5 \Delta \boldsymbol{x}$, respectively.

Note that the mechanical power can be conditioned by a variable blade pitch angle $\beta$ in (18) through a controller with IG speed error $\Delta\omega_r^u$ as the primary stabilizing signal in the output vector in (19).

### *B. Elimination of Steady-State Errors Through the Augmented State Equations*

To ensure zero steady-state errors for load bus voltage $V_L$ and dc-capacitor voltage $v_{\rm dc}$, two integral terms $\int \Delta V_L dt$ and $\int \Delta v_{\rm dc} dt$ are required in addition to the state variables in (14b). Furthermore, the operating point of the IG changes with wind speed and load and different reference values for $\Delta i'_{qe}$ and $\Delta i'_{de}$ may be required by the STATCOM to achieve good regulation of load bus voltage $V_L$ and dc-capacitor voltage $v_{\rm dc}$. In order for the STATCOM currents $\Delta i'_{qe}$ and $\Delta i'_{de}$ to follow the reference values $\Delta i'^*_{qe}$ and $\Delta i'^*_{de}$ and ensure tight regulations for $\delta i'_{qe} = \Delta i'^*_{qe} - \Delta i'_{qe}$ and $\delta i'_{de} = \Delta i'^*_{de} - \Delta i'_{de}$, we need two additional state variables $\int \delta i'_{qe} dt$ and $\int \delta i'_{de} dt$. In the present work, the integral terms $\int\int \Delta V_L dt$ (which is related to $\int \delta i'_{qe} dt$, since $\int \Delta V_L dt$ is proportional to $\Delta i'^*_{qe}$ [4]) and $\int\int \Delta v_{\rm dc}\, dt$ (which is related to $\int \delta i'_{de} dt$, since $\int \Delta v_{\rm dc} dt$ is proportional to $\Delta i'^*_{de}$ [4]) are employed as the additional state variables. With the four integral terms $\int \Delta V_L dt$, $\int \Delta v_{\rm dc} dt$, $\int\int \Delta V_L dt$, and $\int\int \Delta v_{\rm dc} dt$ as the additional state variables, we have the augmented state equations as follows:

$$\begin{aligned} \dot{\Delta}\boldsymbol{x}_a &= \boldsymbol{A}_a \cdot \Delta \boldsymbol{x}_a + \boldsymbol{B}_a \cdot \Delta \boldsymbol{u} \\ \Delta \boldsymbol{y}_a &= \boldsymbol{C}_a \Delta \boldsymbol{x}_a \end{aligned} \tag{20}$$

where

$$\Delta \boldsymbol{x}_a = \begin{bmatrix} \Delta \boldsymbol{x} \\ \Delta \boldsymbol{z} \end{bmatrix}, \quad \Delta \boldsymbol{y}_a = \begin{bmatrix} \Delta \boldsymbol{y} \\ \Delta \boldsymbol{z} \end{bmatrix}$$

$$\Delta \boldsymbol{z} = \begin{bmatrix} \int \Delta V_L dt & \int \Delta v_{\rm dc} dt & \int\int \Delta V_L dt & \int\int \Delta v_{\rm dc} dt \end{bmatrix}^T$$

$$\boldsymbol{A}_a = \begin{bmatrix} \boldsymbol{A} & \boldsymbol{0} & \boldsymbol{0} \\ \boldsymbol{C}_1 & \boldsymbol{0} & \boldsymbol{0} \\ \boldsymbol{C}_2 & \boldsymbol{0} & \boldsymbol{0} \\ \boldsymbol{0} & \boldsymbol{I}_{2\times 2} & \boldsymbol{0} \end{bmatrix}, \quad \boldsymbol{B}_a = \begin{bmatrix} \boldsymbol{B} \\ \boldsymbol{0} \end{bmatrix}, \quad \boldsymbol{C}_a = \begin{bmatrix} \boldsymbol{C} & \boldsymbol{0} \\ \boldsymbol{0} & \boldsymbol{I}_{4\times 4} \end{bmatrix} \tag{21}$$

## IV. Control Design

The main objective of the proposed controller is to regulate certain output measurements and drive system states to equilibrium operating points when the wind-driven induction generator system is subjected to various disturbances under both grid-connection and islanding conditions. In the design of the output feedback controller, the pole placement approach based on linear quadratic control (LQC) will be used. The goals in the controller design process include both transient excursion suppression and good regulations in steady-state operation.

### A. Linear Quadratic State Feedback Control

For the linear system described in (20), the linear quadratic state feedback control $\Delta \boldsymbol{u}$ that minimizes the performance index

$$J = \frac{1}{2}\int_0^\infty \left(\Delta \boldsymbol{x}_a^T \boldsymbol{Q} \Delta \boldsymbol{x}_a + \Delta \boldsymbol{u}^T \boldsymbol{R} \Delta \boldsymbol{u}\right) dt \tag{22}$$

where $\boldsymbol{Q}$ is the weighting matrix of the state variable variations and $\boldsymbol{R}$ that of the control effort, is given by [13]

$$\Delta \boldsymbol{u} = -\boldsymbol{K}_s \Delta \boldsymbol{x}_a. \tag{23}$$

The closed-loop system equation with the optimal control $\Delta \boldsymbol{u}(t)$ is

$$\dot{\Delta}\boldsymbol{x}_a = \boldsymbol{A}_s \Delta \boldsymbol{x}_a, \quad \boldsymbol{A}_s = \boldsymbol{A}_a - \boldsymbol{B}_a \boldsymbol{K}_s = \boldsymbol{A}_a - \boldsymbol{S}\boldsymbol{M} \tag{24}$$

where

$$\begin{aligned} \boldsymbol{S} &= \boldsymbol{B}_a \boldsymbol{R}^{-1} \boldsymbol{B}_a^T \\ \boldsymbol{K}_s &= \boldsymbol{R}^{-1} \boldsymbol{B}_a^T \boldsymbol{M} \end{aligned} \tag{25}$$

and $\boldsymbol{M}_s$ is the positive semidefinite (stabilizing) solution $\boldsymbol{M}$ of the algebraic Riccati equation (ARE)

$$\boldsymbol{A}_a^T \boldsymbol{M} + \boldsymbol{M}\boldsymbol{A}_a + \boldsymbol{Q} - \boldsymbol{M}\boldsymbol{S}\boldsymbol{M} = \boldsymbol{0}. \tag{26}$$

To determine the state feedback gain matrix $\boldsymbol{K}_s$ for the linear quadratic control in (23), a set of initial weights $q_{ij}^{(0)}$ must be first chosen for the weighting matrix $\boldsymbol{Q}$ in (22) based on physical reasoning and past experience. In the present work, a diagonal weighting matrix with the diagonal elements 10, 0, 0, 1, 100, 100, 1, and 1 corresponding to the state variables $\Delta v_{\rm dc}$, $\Delta i_{de}$, $\Delta i_{qe}$, $\Delta \omega_r^u$, $\int \Delta V_L\, dt$, $\int \Delta v_{\rm dc} dt$, $\int\int \Delta V_L\, dt$, and $\int\int \Delta v_{\rm dc}\, dt$, respectively, is selected as the initial weighting matrix. The weights for the other state variables of minor concern are chosen to be zero. Note that the weights for STATCOM currents $\Delta i_{de}$ and $\Delta i_{qe}$ have been chosen to be small (zero) because it may be necessary to adjust these variables to new values in order to regulate load bus voltage under various disturbances. Higher but moderate weights are placed on the integral terms $\int \Delta V_L\, dt$, $\int \Delta v_{\rm dc}\, dt$ to avoid steady-state errors in load bus voltage and dc-capacitor voltage. However, if an extremely high weight is placed on these variables, the adjustment in the reference currents ($\Delta i_{qe}^{\prime *}$ and $\Delta i_{de}^{\prime *}$) may be limited by the control laws which tries to keep the integral terms fixed at their original values in order to minimize the state variations. With the weighting matrices at hand, we can proceed to determine the feedback gain matrix $\boldsymbol{K}_s$ using (25).

If the dampings for the closed-loop eigenvalues with the optimal control in (23) are not satisfactory, the initial weighting matrix may be updated using the pole placement technique in [14], where procedures have been described to move the closed-loop eigenvalues by introducing a degree of relative stability $\chi$ into the original performance criterion and modifying the weighting matrix $\boldsymbol{Q}$. Then the new spectrum (the collections of stable eigenvalues) $\boldsymbol{\Lambda}$ of the optimal system with the modified weighting matrix $(\boldsymbol{Q} - 2\chi \boldsymbol{M}_u)$ is

$$\boldsymbol{\Lambda} = \boldsymbol{\Lambda}_s - 2\chi \boldsymbol{I} \tag{27}$$

where $\boldsymbol{M}_u$ is the negative semidefinite solution $\boldsymbol{M}$ of (26), and $\boldsymbol{\Lambda}_s$ is the spectrum of the optimal system with the initial weighting matrix.

To determine $\boldsymbol{M}_u$, we assume that $(\boldsymbol{A}_a, \boldsymbol{B}_a)$ is stabilizable and the Hamiltonian matrix

$$\boldsymbol{H}_0 = \begin{bmatrix} \boldsymbol{A}_a & -\boldsymbol{S} \\ -\boldsymbol{Q} & -\boldsymbol{A}_a^T \end{bmatrix}$$

has no pure imaginary eigenvalues. These conditions are necessary and sufficient to ensure the existence of a unique matrix $\boldsymbol{M}_s \stackrel{\geq}{=} 0$ such that (24) is stable. The closed-loop eigenstructure can be written as Jordan decomposition of $\boldsymbol{H}_0$ in the form [14], [15]

$$\begin{bmatrix} \boldsymbol{A}_a & -\boldsymbol{S} \\ -\boldsymbol{Q} & -\boldsymbol{A}_a^T \end{bmatrix} \begin{bmatrix} \boldsymbol{X_0} & \boldsymbol{W_0} \\ \boldsymbol{Y_0} & \boldsymbol{Z_0} \end{bmatrix} = \begin{bmatrix} \boldsymbol{X_0} & \boldsymbol{W_0} \\ \boldsymbol{Y_0} & \boldsymbol{Z_0} \end{bmatrix} \begin{bmatrix} \boldsymbol{\Lambda}_s & \boldsymbol{0} \\ \boldsymbol{0} & \boldsymbol{\Lambda}_u \end{bmatrix} \tag{28}$$

where $\boldsymbol{\Lambda}_s$ and $\boldsymbol{\Lambda}_u$ are the collections of the stable and unstable eigenvalues of $\boldsymbol{H}_0$, respectively. Note that $\boldsymbol{\Lambda}_s$ and $\boldsymbol{\Lambda}_u$ are symmetric with each other with respect to the imaginary axis. The matrix $\boldsymbol{M}_s$ can be derived from the eigenvectors of $\boldsymbol{H}_0$ associated with the stable eigenvalues in (28) in the form

$$\boldsymbol{M}_s = \boldsymbol{Y}_0 \boldsymbol{X}_0^{-1}. \tag{29}$$

Similarly, a negative semidefinite matrix

$$\boldsymbol{M}_u = \boldsymbol{Z}_0 \boldsymbol{W}_0^{-1} \tag{30}$$

exists and is also a solution of the ARE in (26) associated with the unstable eigenvalues.

The results of [14] allow a desired shift in the locations of the original eigenvalues by using a negative semidefinite matrix $(\boldsymbol{M}_u)$ that is obtained from the initial weighting matrix. It is noted that partial placement of optimal eigenvalues can be reached in the same manner and will be used in this paper.

### B. Output Feedback Control

Since some state variables such as $\Delta \phi_{qr}, \Delta \phi_{dr}, \Delta \phi_{qs}$, and $\Delta \phi_{ds}$ are not readily measurable, nine output variables $\Delta V_L$, $\Delta v_{\rm dc}$, $\Delta \omega_r^u$, $\Delta i'_{qe}$, $\Delta i'_{de}$, $\int \Delta V_L dt$, $\int \Delta v_{\rm dc} dt$, $\int\int \Delta V_L dt$, and $\int\int \Delta v_{\rm dc} dt$ as listed in (21) are selected to be the feedback signals. Then, the output feedback control $\Delta \boldsymbol{u}$ is given by

$$\Delta \boldsymbol{u} = -\boldsymbol{K}_{\rm o} \Delta \boldsymbol{y}_a \tag{31}$$

TABLE I
SUMMARY OF SYSTEM EIGENVALUES

| Open-loop eigenvalues | Closed-loop eigenvalues | |
|---|---|---|
| | State feedback | Output feedback |
| *Generator Dynamics* | *Generator Dynamics* | |
| −123.83± j2340.2 | −124.73± j2340.9 | −124.63± j2357.2 |
| −5.79± j7.94* | −17.79± j7.91* | −9.61± j6.17* |
| −12.93 | −12.83 | −7.60 |
| *STATCOM Dynamics* | *STATCOM Dynamics* | |
| −45.68± j376.44@ | −261.53± j530.26@ | −97.29± j553.17@ |
| −0.07739 | −539.5 | −579.5 |
| *Controller Dynamics* | *Controller Dynamics* | |
| 0 | −10.20 | −11.31± j0.93 |
| 0 | −11.005 | |
| 0 | −11.899 | −21.17± j15.38 |
| 0 | −11.9 | |

* electromechanical mode; at the ac current mode of STATCOM.

where the output feedback gain matrix $\boldsymbol{K}_{\rm o}$ is related to the state feedback gain matrix $\boldsymbol{K}_s$ as follows:

$$\boldsymbol{K}_{\rm o}\boldsymbol{C}_a = \boldsymbol{K}_s. \tag{32}$$

Thus, the output feedback gain matrix $\boldsymbol{K}_{\rm o}$ can be derived using $\boldsymbol{K}_s$ and $\boldsymbol{C}_a^{\dagger}$, the pseudoinverse [9], [16] of the augmented output matrix $\boldsymbol{C}_a$, as follows:

$$\boldsymbol{K}_{\rm o} = \boldsymbol{K}_s\boldsymbol{C}_a^{\dagger} \tag{33}$$

where

$$\boldsymbol{C}_a^{\dagger} = \boldsymbol{C}_a^T\left(\boldsymbol{C}_a\boldsymbol{C}_a^T\right)^{-1}.$$

Sets of open-loop and closed-loop eigenvalues for the WECS are summarized in Table I. The relative stability of $\chi = 6$ is introduced to shift the eigenvalues for the electromechanical mode from $-5.79 \pm j7.94$ to $-17.79 \pm j7.91$ in order to improve the damping effect for the closed-loop system with state feedback controller. On the other hand, the eigenvalues for the electromechanical mode are shifted to new locations $-9.61 \pm j6.17$ if an output feedback controller with generator speed feedback and pitch angle control is used. In this case, the diagonal elements of the modified state weighting matrix corresponding to $\Delta v_{\rm dc}$, $\Delta i_{de}$, $\Delta i_{qe}$, $\Delta\omega_r^u$, $\int \Delta V_L$, $\int \Delta v_{\rm dc}$, $\int\int \Delta V_L$, and $\int\int \Delta v_{\rm dc}$ become 9.46, 0.00018, 0.00024, 53221, 207.65, 557.77, 197.88, and 205.28, respectively. It is clear that the modified weight on $\Delta\omega_r^u$ is higher than that of the initial weight since improved damping for the electromechanical mode is desired. In addition, in the grid-connection condition, a poorly damped STATCOM mode characterized by the pair of eigenvalues $-45.68 \pm j376.44$ is present in the open-loop response. This mode can be shifted by the output feedback controller to the new locations $-97.29 \pm j553.17$. Moreover, the pair of well-damped modes for controller dynamics in Table I indicate that the deviations of load bus voltage and dc-capacitor voltage would be reduced by the proposed output feedback controller.

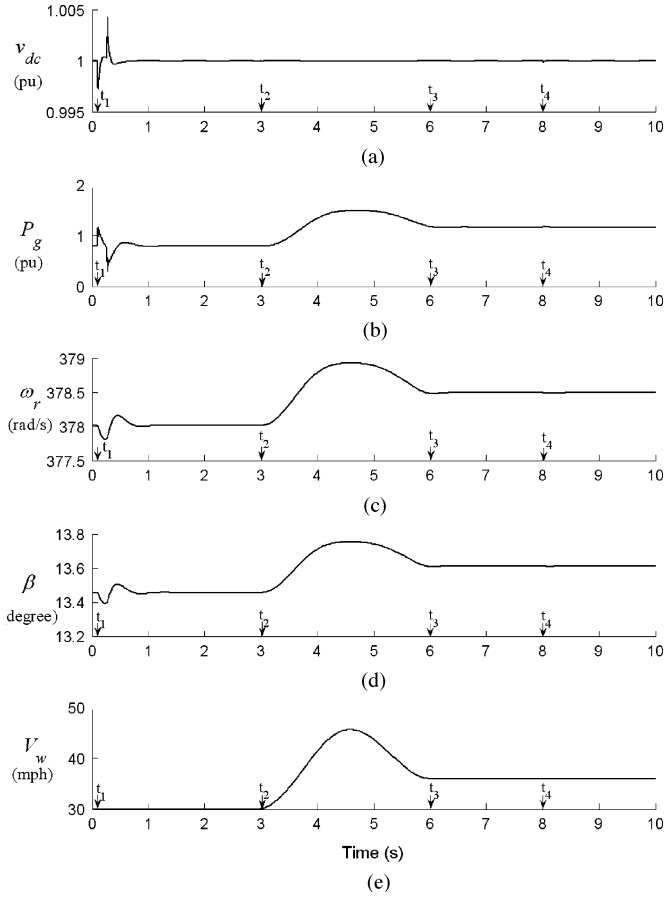


Fig. 5. Dynamic responses for the WECS operated in grid-connection condition. (A 10-cycle temporary voltage dip of 5% at grid began at $t_1 = 0.095$ s). (Wind gust began at $t_2 = 3.0$ s). (Wind gust ended at $t_3 = 6.0$ s). (A step load change of 10% began at $t_4 = 8.0$ s).

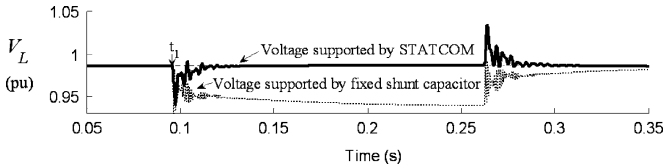


Fig. 6. Dynamic responses for load bus voltage when the WECS was operated in grid-connection condition. (A temporary voltage dip of 5% at grid began at $t_1 = 0.095$ s).

## V. SIMULATION RESULTS

### A. Grid-Connection Performance

The dynamic performances of the output feedback controller for the WECS were examined under three successive disturbances and the results are depicted in Figs. 5–8. The first event was a temporary voltage dip of 5% at the grid bus starting at $t_1 = 0.095$ s and lasting for ten cycles. The voltage dip caused a transient swing of $\pm 0.2$ rad/s in generator speed, as shown in Fig. 5(c). The response curves in Fig. 5(c) and (d) reveal that the blade pitch angle can be controlled to limit generator speed deviation in this event.

The second disturbance of a wind gust started at $t_2 = 3.0$ s, reaching the peak wind speed of 46 mph at $t = 4.6$ s, and finally the wind speed dropped to 36 mph at $t_3 = 6.0$ s. For the

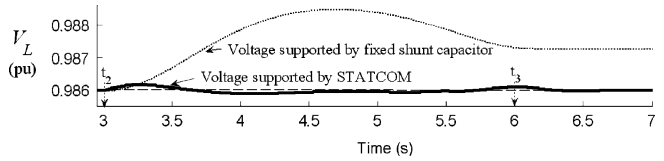


Fig. 7. Dynamic responses for load bus voltage when the WECS was operated in grid-connection condition. (Wind gust began at $t_2 = 3.0$ s). (Wind gust ended at $t_3 = 6.0$ s).

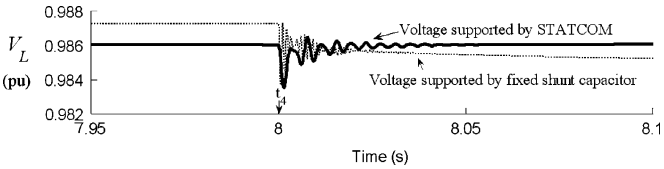


Fig. 8. Dynamic responses for load bus voltage when the WECS was operated in grid-connection condition. (A step load change of 10% began at $t_4 = 8.0$ s).

sake of clarity, the effects of wind shear and tower shadow were ignored. It is obvious that the rotor would accelerate as a result of the increasing mechanical power caused by increasing wind speed if the pitch angle was fixed. However, as demonstrated in Fig. 5(d), the wind-sensorless output feedback controller generated a pitch angle command as soon as the wind speed began to increase. In addition, the increased output power converted from aerodynamic power after gust was another benefit of the controller, as illustrated in Fig. 5(b). The third disturbance considered was a 10% step change in load demand that took place at $t_4 = 8.0$ s. This sudden increase in load demand caused a transient drop in the kinetic energy and speed of the IG in order to provide the sudden increase in generator output power, as shown in Fig. 5(b) and (c). After this transient, the increase in load power was balanced by the grid, and generator speed returned to its original value as shown in Fig. 5(c). It is also observed from Fig. 5(d) that the pitch angle decreased slightly during the transient and returned to the original value afterward.

An observation of the response curve in Fig. 5(a) indicates that the dc-capacitor voltage can be kept almost constant under these disturbances except for a very small deviation of $\pm 0.4\%$ in the voltage dip event.

It is also observed from the response curves in Figs. 6–8 that the STATCOM with the output feedback controller is superior to the fixed shunt capacitor in providing voltage support for the WECS under large disturbances. As illustrated in Fig. 6, the load bus voltage supported by STATCOM settled to the steady-state value in 2 cycles after the sudden change in grid voltage. Besides, it is clear that a very small transient excursion of $\pm 0.015\%$ in load bus voltage was observed during the wind gust transient, as shown in Fig. 7. A transient excursion of less than 0.3% and lasting for only 2 cycles is observed for the load bus voltage in Fig. 8 when the system was subjected to a step load change. In contrast to the STATCOM, the voltage supported by the fixed shunt capacitor experienced considerably higher voltage excursions and steady-state errors, as shown in Figs. 6–8.

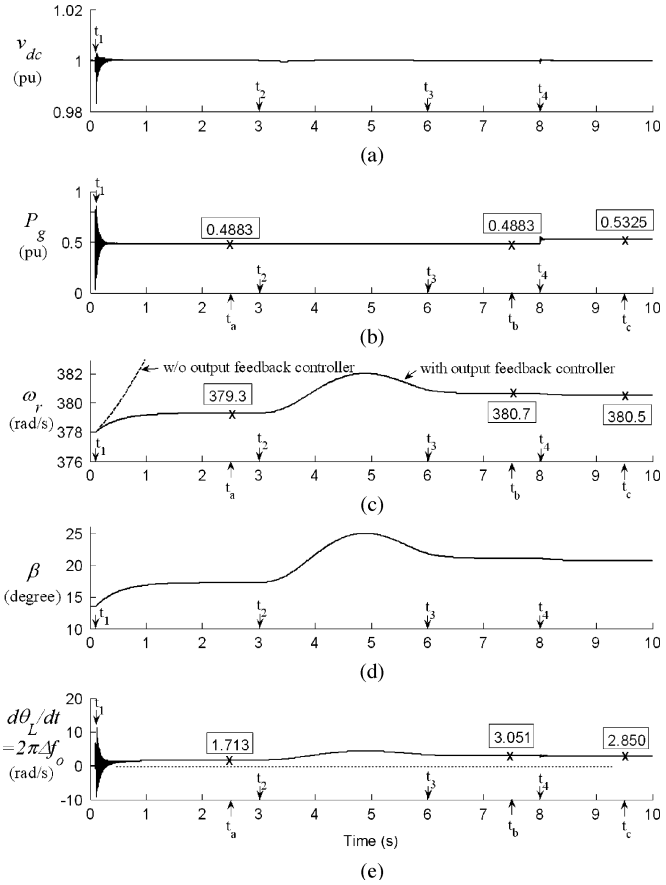


Fig. 9. Dynamic responses for the WECS operated in islanding condition. (Grid disconnection began at $t_1 = 0.095$ s). (Wind gust began at $t_2 = 3.0$ s). (Wind gust ended at $t_3 = 6.0$ s). (A step load change of 10% began at $t_4 = 8.0$ s).

### B. Islanding Performance

Self-excitation can occur if the IG loses its connection to the grid. Unstable voltage and frequency may be observed during self-excitation [7], [8]. In the first simulated event, the WECS lost its connection to the grid at $t_1 = 0.095$ s and remained in islanding mode thereafter. Fig. 9(b) illustrates that the output power of IG dropped rapidly from 0.798 to 0.488 p.u. after the grid-disconnection transient since the IG exported a real power of 0.31 p.u. to the grid before it was disconnected from the grid. Note that the load demand remained unchanged when the IG was disconnected from the grid since the load bus voltage magnitude was fixed by the STATCOM at steady state. This is as expected since constant impedance load model was employed in this simulation. During the grid-disconnection transient, the surplus mechanical power resulting from the decrease in electrical power output was conditioned by increasing the blade pitch angle $\beta$. Generator speed can thus be stabilized to a new value, as shown in Fig. 9(c) and (d). The frequency difference $\Delta f_o$ (Hz) between the grid and the islanding induction generator is depicted as the rate of change in angular displacement ($d\theta_L/dt$, which is equal to $2\pi\Delta f_o$ in rad/s) in Fig. 9(e). It is observed from Fig. 3 that the $\theta_L$, the relative angular displacement between the vectors of load bus voltage $\boldsymbol{V}_L$ and the grid bus voltage $\boldsymbol{V}_\infty$,

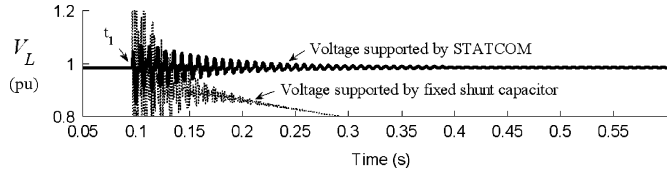


Fig. 10. Dynamic responses for load bus voltage when the WECS was operated in islanding condition. (Grid disconnection began at $t_1 = 0.095$ s).

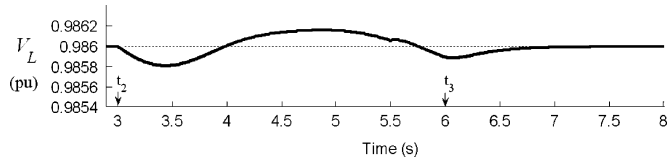


Fig. 11. Dynamic responses for load bus voltage when the WECS was operated in islanding condition. (Wind gust began at $t_2 = 3.0$ s). (Wind gust ended at $t_3 = 6.0$ s).

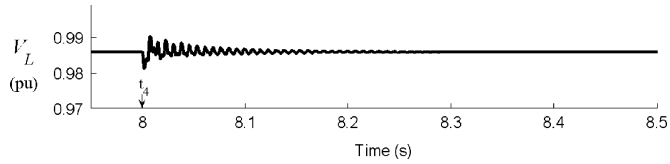


Fig. 12. Dynamic responses for load bus voltage when the WECS was operated in islanding condition. (A step load change of 10% began at $t_4 = 8.0$ s).

can not be fixed since the load bus voltage vector $\boldsymbol{V}_L$ rotates at a speed $\omega$ that is different from the synchronous speed $\omega_s$ for the grid voltage vector $\boldsymbol{V}_\infty$ under islanding condition. Thus $d\theta_L/dt$ no longer equaled zero and there was a frequency difference between the islanding IG and the grid.

When the WECS was operated under islanding condition, a wind gust and a step load change of 10% were assumed to take place at $t_2 = 3.0$ s and $t_4 = 8.0$ s, respectively, in order to examine the dynamic performance of the output feedback controller under disturbance conditions. It is observed from Fig. 9(c) and (e) that both generator speed $(\omega_r)$ and the rate of change of relative angular displacement $(d\theta_L/dt)$ can be stabilized to new equilibrium points by the control of blade pitch angle $\beta$ [Fig. 9(d)] under islanding condition.

As shown in Fig. 9(a), the dc-capacitor voltage can be kept almost constant under all disturbances except for a small transient excursion of 1.8% during the grid-disconnection event.

Figs. 10–12 summarize the voltage regulation performances of output feedback controller for the WECS in islanding condition. As illustrated in Fig. 10, the load bus voltage settled to a steady-state value in 10 cycles during the grid-disconnection transient. Figs. 11 and 12 show that the transient excursions in load bus voltage can be suppressed to be less than $\pm 0.02\%$ and $\pm 1\%$ by the controller for the disturbances of wind gust and sudden change in load, respectively. Besides, undervoltage (underexcitation) may occur due to insufficient reactive power compensation by fixed shunt capacitor for the IG when it is disconnected from the grid, as illustrated in Fig. 10.

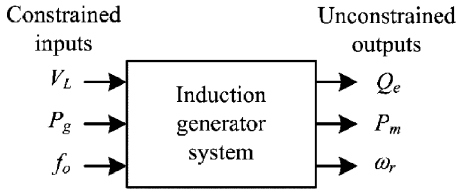


Fig. 13. Induction generator input–output variables for steady-state analysis in islanding.

## VI. Steady-State Analysis for Frequency Control of an Isolated Induction Generator

It has been observed from the response curve in Fig. 9(e) that system frequency no longer remained fixed at the rated value of 60 Hz when the induction generator was disconnected from the power grid and was operated under islanding condition. In fact, frequency deviations of 0.485 Hz (3.051 rad/s) and 0.454 Hz (2.850 rad/s) were observed for the isolated generator when it was subjected to wind gust and a step load change, respectively. Under the assumption of sufficient mechanical power input, it is interesting to study how to reduce the frequency deviations and maintain constant frequency operation for an isolated induction generator. To do this, the relationship between rotating speed $(\omega_r)$ and real power output $(P_g)$ at various frequencies for the isolated induction generator under steady-state operating condition must be first determined.

### *A. Algorithm for Determining the Steady-State Operating Points of an Isolated Induction Generator*

To find the steady-state operating points for an isolated induction generator with a shunt excitation capacitor, an iterative approach has been proposed [3] to solve the nodal equations for the induction generator system. However, it is difficult to formulate nodal equations for an IG with a voltage regulator. In this paper, a simple steady-state analysis algorithm based on dynamic system model is proposed for an isolated IG with a voltage regulator using the MATLAB function TRIM. The voltage regulator can be a STATCOM, an SVC, or a capacitor with adjustable capacity. As shown in Fig. 13, the constrained inputs to the induction generator system include load bus voltage $V_L$, generator output $P_g$, and system frequency $f_o$. The unconstrained outputs include mechanical power $P_m$, generator speed $\omega_r$, and the required reactive power $Q_e$. Fig. 14 depicts the flow chart for the proposed steady-state analysis algorithm. In the algorithm, proper capacity of the equivalent shunt capacitor can be determined such that the load bus voltage $V_L$ is fixed at 0.986 p.u. The generator speed $\omega_r$ is computed for various combinations of electrical output power $P_g$ and system frequency $f_o$ using the power repetition loop and the frequency repetition loop in Fig. 14. Note that the equivalent load impedance must be updated in the power repetition loop when the constrained generator output power is changed. In addition, the angular speed $\omega_s$ for the synchronous reference frame and the base quantity $\omega_b$ must be set to be equal to the specified frequency $2\pi f_o$ in the frequency repetition loop. The per unit reactance, inertia

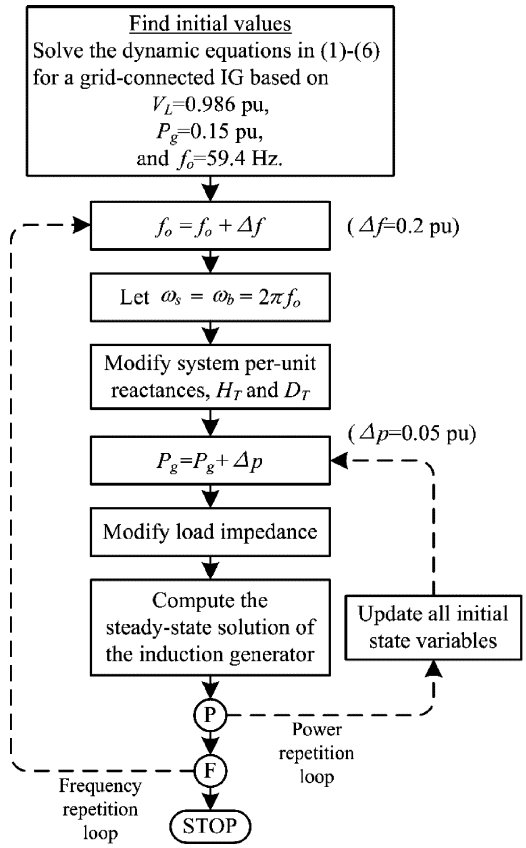


Fig. 14. Flow chart for the proposed steady-state analysis algorithm for an IG operated in islanding.

constant $H_T$ and damping constant $D_T$ must also be updated based on the specified frequency $2\pi f_{\rm o}$.

Since the nonlinear induction generator model has more than one steady-state solution, the reasonable steady-state solution hinges on the initial value. To acquire reasonable steady-state solution and speed up convergence while using the proposed algorithm, the first initial condition can be obtained by solving the dynamic equations of grid-connected IG since the output frequency is the same as the grid frequency at steady-state, irrespective of generator speed or load power, thus confining the solution to a small region. In addition, steady-state solution in each power repetition loop can be treated as the initial value for the next power repetition loop to speed up convergence, as shown in Fig. 14.

Fig. 15 shows the results from steady-state analysis for output frequencies $f_{\rm o}$ ranging from 59.4 to 60.6 in 0.2-Hz increment with the load bus voltage fixed at 0.986 p.u. It is observed from Fig. 15 that generator speed $\omega_r$ increases linearly with increasing real power output $P_g$ at a specific output frequency. It is also observed that a change in output frequency means a change in rotor speed when the real power output is held constant.

Note that the steady-state operating points at $t_a = 2.5$ s, $t_b = 7.5$ s, and $t_c = 9.5$ s in Fig. 9 are marked in Fig. 15. The corresponding frequency deviations for the three operating points in Fig. 15 are 0.272 Hz (1.713 rad/s), 0.485 Hz (3.051 rad/s), and 0.454 Hz (2.850 rad/s), respectively, which match closely with the dynamic simulation results in Fig. 9(e).

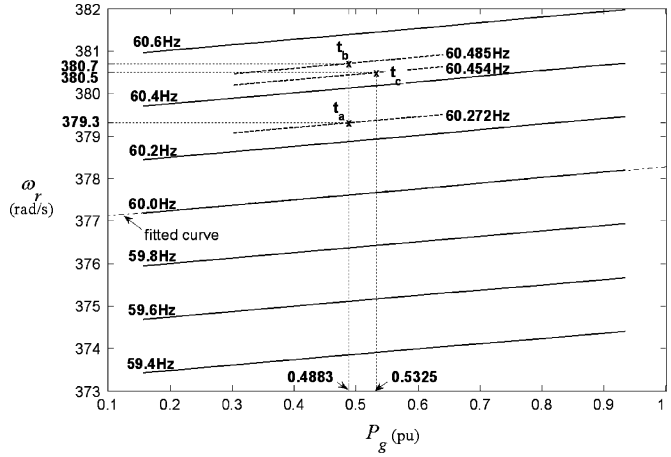


Fig. 15. Rotating speed ($\omega_r$) versus real power output ($P_g$) at different frequencies for an isolated IG.

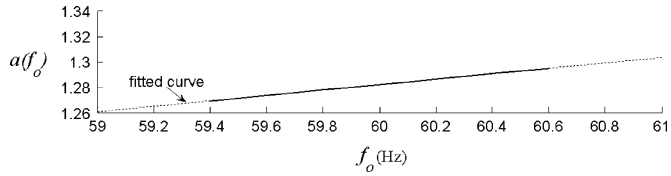


Fig. 16. Slope variation of $P_g$ versus $\omega_r$ curve with various output frequencies.

### B. Constant Frequency Controller Design

Fig. 15 gives the relationship between generator speed $\omega_r$, frequency $f_{\rm o}$, and real power output $P_g$ for an islanding IG under constant voltage control. An interesting application of the steady-state operating characteristics in Fig. 15 would be the constant frequency operating mode for an induction generator with sufficient mechanical power $P_m$. In the design of a constant frequency controller for such an isolated IG, the generator speed $\omega_r$ in Fig. 15 is first expressed as a linear function of its real power output $P_g$:

$$\omega_r|_{f_{\rm o}} = \Omega(P_g) = aP_g + b \quad \text{(rad/s)}. \tag{34}$$

Since the IG delivers zero output power when it is operated at synchronous rotating speed ($\omega_r = 2\pi f_{\rm o}$), the parameter $b$ in (34) equals the synchronous frequency $2\pi f_{\rm o}$. In addition, the slope $a$ in (34) at each frequency $f_{\rm o}$ can be measured from the curves in Fig. 15 and is plotted in Fig. 16. It is observed from Fig. 16 that the slope $a$ can be approximated as a linear function of $f_{\rm o}$ as follows:

$$a(f_{\rm o}) = 0.02125 f_{\rm o} + 0.0071. \tag{35}$$

Substituting (35) into (34) yields the general form for the reference rotor speed in terms of the actual real-power output and the specified output frequency as

$$\omega_r^* = \Omega^*(P_g, f_{\rm o}^*) = a(f_{\rm o}^*)P_g + 2\pi f_{\rm o}^* \quad \text{(rad/s)}. \tag{36}$$

Based on (36), a proportional-integral controller as shown in Fig. 17 is proposed to reach constant frequency control for an isolated induction generator. As shown in Fig. 17, the inputs to the proposed constant frequency controller are the desired frequency $f_{\rm o}^*$ ($f_{\rm o}^* = 60$ Hz in this work), the real power output

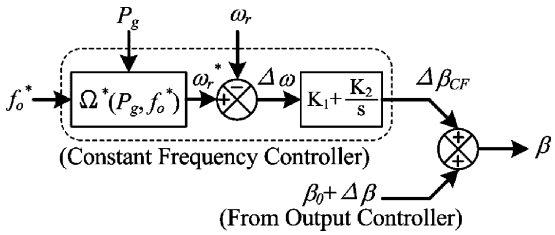


Fig. 17. Constant frequency controller for an IG operated in islanding condition.

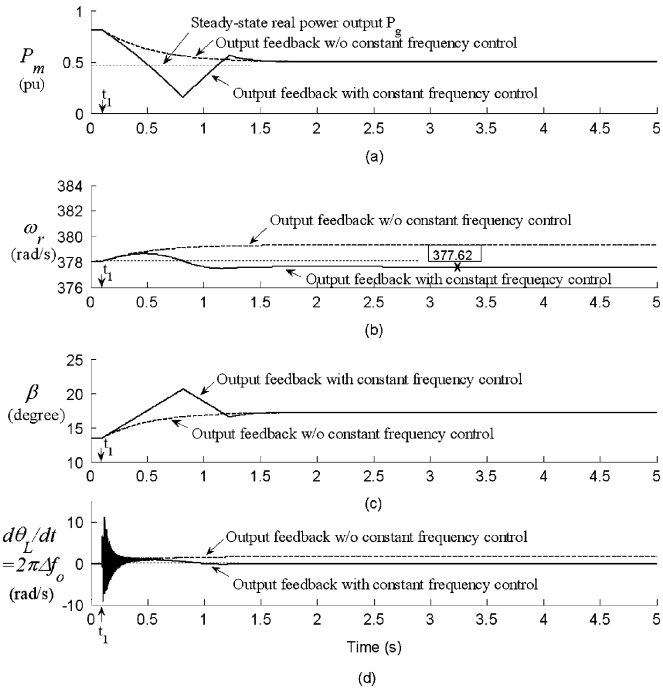


Fig. 18. Dynamic responses for the wind-driven IG with constant frequency controller and without constant frequency controller. (Grid disconnection began at $t_1 = 0.095$ s).

$P_g$, and the generator speed $\omega_r$. The reference speed $\omega_r^*$ is determined using (36). When the actual speed $\omega_r$ deviates from the reference speed $\omega_r^*$ (e.g., $\omega_r > \omega_r^*$), then the PI controller generates the desired pitch angle command $\Delta\beta_{CF}$ based on the speed deviation $(\Delta\omega = \omega_r^* - \omega_r)$. A negative $\Delta\omega$ causes an increase in pitch angle $(\Delta\beta_{CF} > 0)$. As a result, the mechanical power input to the generator is decreased, causing a decrease in the kinetic energy and rotating speed of the generator. Finally, the rotating speed $\omega_r$ settles down to a lower steady-state value and the frequency deviation is eliminated.

To examine the effectiveness of the proposed constant frequency controller, dynamic responses for the induction generator that was disconnected from the grid at $t_1 = 0.095$ s are depicted in Fig. 18. It is observed from Fig. 18(d) that zero-frequency deviation $(d\theta_L/dt = 2\pi\Delta f_o = 0)$ can be reached by the proposed constant frequency controller. This is achieved by increasing the pitch angle $\beta$, causing a temporary decrease in mechanical power $P_m$ and a decrease in generator speed $\omega_r$, as shown in Fig. 18(a)–(c). For comparison, the generator speed $\omega_r$ for the output feedback without constant frequency control is also shown in Fig. 18(b). It can be observed that the output feedback controller without constant frequency control can provide stable operation with satisfactory response under islanding operation except for a small frequency deviation as shown in Fig. 18(d). This means that the mechanical power $P_m$, during the grid-disconnection transient, was controlled to be slightly higher than the real-power output $P_g$ so that the accumulated kinetic energy accelerated IG to a higher rotating speed, as illustrated in Fig. 18(a) and (b).

Another important application of (36) is the design of a constant output power controller for the IG connected with a grid. In this case, the generator speed reference $\omega_r^*$ is derived based on the desired real power output $P_g^*$ and system frequency $f_o$, as shown in Fig. 17.

## VII. Conclusion

A STATCOM and blade pitch control system has been successfully designed to regulate the load bus voltage and stabilize rotor speed for an induction generator in a variable-speed WECS. A major feature of the present work is that the two-reference-frame model is included in the detailed dynamic system model in order to achieve decoupled control for the STATCOM real and reactive power control loops. Besides, a systematic approach based on pole placement technique has been developed to determine proper weighting matrix for the linear quadratic controller such that the eigenvalues for the closed-loop system can be shifted to desired locations.

To ensure zero steady-state error regulation and improve transient excursion for load bus voltage and dc-capacitor voltage, four new states, $\int \Delta V_L\, dt, \int \Delta v_{\rm dc}\, dt, \iint \Delta V_L\, dt$, and $\iint \Delta v_{\rm dc}\, dt$, have been augmented in the system dynamic model. Simulation results indicate that the output feedback controller designed for the STATCOM and blade pitch is capable of improving WECS dynamic responses in case of disturbances under grid-connection or islanding conditions. It is also noted that generator speed feedback instead of wind speed feedback for the output feedback controller provides satisfactory transient response in stabilizing generator speed. A simple algorithm based on dynamic system model for an isolated IG has been developed such that a flexible steady-state analysis is achievable under various operating conditions. Utilizing the steady-state properties deduced by means of the proposed algorithm, a proportional-integral controller has been designed such that constant frequency operation (for an isolated IG) and constant-output power operation (for a grid-connected IG) can both be reached as long as the mechanical power is sufficient. The proposed constant output frequency controller and constant output power controller are also suitable for applications in hydro-driven or steam-driven induction generator systems.

## Appendix

*1) Fixed Shunt Capacitor Model:*

$$\dot{v}_{dL} = \omega_s v_{qL} + \omega_b X_c i_{d\rm FC}$$
$$\dot{v}_{qL} = -\omega_s v_{dL} + \omega_b X_c i_{q\rm FC}.$$

*2) Transmission Line Model:*

$$\dot{i}_{d\mathrm{TL}} = -\frac{\omega_b r_{\mathrm{TL}}}{X_{\mathrm{TL}}} i_{d\mathrm{TL}} + \omega_s i_{q\mathrm{TL}} + \frac{\omega_b}{X_{\mathrm{TL}}}(v_{dL} - v_{d\infty})$$

$$\dot{i}_{q\mathrm{TL}} = -\frac{\omega_b r_{\mathrm{TL}}}{X_{\mathrm{TL}}} i_{q\mathrm{TL}} - \omega_s i_{d\mathrm{TL}} + \frac{\omega_b}{X_{\mathrm{TL}}}(v_{qL} - v_{q\infty}).$$

*3) Load Model:*

$$\dot{i}_{dL} = -\frac{\omega_b r_L}{X_L} i_{dL} + \omega_s i_{qL} + \frac{\omega_b}{X_L} v_{dL}$$

$$\dot{i}_{qL} = -\frac{\omega_b r_L}{X_L} i_{qL} - \omega_s i_{dL} + \frac{\omega_b}{X_L} v_{qL}.$$

*4) Simulation Parameters:*

| Induction Generator (2.5MW, 4 poles, 4.16kV, 60Hz ) | | |
|---|---|---|
| Stator resistance | $r_s$ | 0.0042 pu |
| Rotor resistance | $r_r$ | 0.0032 pu |
| Stator leakage reactance | $X_s$ | 0.0326 pu |
| Rotor leakage reactance | $X_r$ | 0.0326 pu |
| Fixed shunt capacitor reactance | $X_c$ | 3.0 pu |
| Saturation parameters | | |
| Air gap voltage $V_g$ (pu) | 0.0 0.84 0.86 0.90 0.96 1.06 1.18 1.32 1.44 | |
| Magnetizing reactance $X_m$ (pu) | 1.88 1.88 1.86 1.77 1.63 1.37 1.08 0.77 0.55 | |
| Voltage-Sourced Inverter | | |
| Series line resistance | $r_f$ | 0.02 pu |
| Series line reactance | $X_f$ | 0.14 pu |
| DC-link capacitance | $C_{dc}$ | 2800 μF |
| Switching loss resistance | $r_{dc}$ | 500 pu |
| Transmission Line | | |
| Line resistance | $r_{TL}$ | 0.015 pu |
| Line reactance | $X_{TL}$ | 0.15 pu |
| Infinite-bus voltage | $V_\infty$ | $1\angle 0^\circ$ pu |
| Load Model | | |
| Nominal power at nominal voltage | $P_L / Q_L$ | 0.6 pu / 0.15 pu |
| Wind Turbine [11], [12] | | |
| Equivalent inertia constant | $H_T$ | 18.711 s |
| Equivalent damping constant | $D_T$ | 0.010125 pu |
| Rotor radius ($A=\pi R^2$) | $R$ | 150 ft |
| Gear ratio | $GR$ | 102.56 |
| System Base Setting | | |
| System MVA | $S_b$ | 2.5MVA |
| Induction generator voltage base | $V_{ACb}$ | $\sqrt{(2/3)}$×4.16kV |
| Inverter DC-link voltage base | $V_{DCb}$ | 2×$V_{ACb}$ |

## REFERENCES


[1] A. Murdoch, R. S. Barton, J. R. Winkelman, and S. H. Javid, "Control design and performance analysis of a 6 MW wind turbine-generator," *IEEE Trans. Power App. Syst.*, vol. PAS-102, no. 5, pp. 1340–1347, Dec. 1983.

[2] L. L. Freris, *Wind Energy Conversion Systems*. Englewood Cliffs, NJ: Prentice-Hall, 1990.

[3] S. S. Murthy, O. P. Malik, and A. K. Tandon, "Analysis of self-excited induction generators," *Proc. Inst. Elect. Eng.–C*, vol. 129, no. 6, pp. 260–265, Nov. 1982.

[4] C. D. Schauder and H. Mehta, "Vector analysis and control of advanced static VAR compensators," *Proc. Inst. Elect. Eng.–C*, vol. 140, no. 4, pp. 299–306, Jul. 1993.

[5] C. T. Chang and Y. Y. Hsu, "Design of UPFC controllers and supplementary damping controller for power transmission control and stability enhancement of a longitudinal power system," *Proc. IEE–Gener. Transm. Distrib.*, vol. 149, no. 4, pp. 463–471, Jul. 2002.

[6] W. L. Chen and Y. Y. Hsu, "Direct output voltage control of a static synchronous compensator using current sensorless d–q vector-based power balancing scheme," in *Proc. IEEE/PES T&D Summer Meet.*, 2003, vol. 2, pp. 545–549.

[7] Z. Saad-Saoud, M. L. Lisboa, J. B. Ekanayake, N. Jenkins, and G. Strbac, "Application of STATCOMs to wind farms," *Proc. IEE–Gener. Transm. Distrib.*, vol. 145, no. 5, pp. 511–516, Sep. 1998.

[8] W. L. Chen and Y. Y. Hsu, "A novel active voltage and frequency regulator to improve grid-disconnection transients of self-excited induction generator system," in *Proc. 5th IEEE Int. Conf. Power Electron. Drive Syst.*, 2003, vol. 2, pp. 1586–1590.

[9] E. S. Abdin and W. Xu, "Control design and dynamic performance analysis of a wind turbine-induction generator unit," *IEEE Trans. Energy Convers.*, vol. 15, no. 1, pp. 91–96, Mar. 2000.

[10] C. M. Ong, *Dynamic Simulation of Electric Machinery Using MATLAB/SIMULINK*. Englewood Cliffs, NJ: Prentice-Hall, 1998.

[11] P. M. Anderson and A. Bose, "Stability simulation of wind turbine systems," *IEEE Trans. Power App. Syst.*, vol. PAS-102, no. 12, pp. 3791–3795, Dec. 1983.

[12] O. Wasynczuk, D. T. Man, and J. P. Sullivan, "Dynamic behavior of a class of wind turbine generators during random wind fluctuations," *IEEE Trans. Power App. Syst.*, vol. 100, no. 6, pp. 2837–2845, Jun. 1981.

[13] F. L. Lewis and V. L. Syrmos, *Optimal Control*. New York: Wiley, 1995.

[14] J. Medanic, H. S. Tharp, and W. R. Perkins, "Pole placement by performance criterion modification," *IEEE Trans. Autom. Control*, vol. 33, no. 5, pp. 469–472, May 1988.

[15] J. C. Willems, "Least squares stationary optimal control and the algebraic Riccati equation," *IEEE Trans. Autom. Control*, vol. 16, no. 6, pp. 621–634, Dec. 1971.

[16] P. H. Huang and Y. Y. Hsu, "An output feedback controller for a synchronous generator," *IEEE Trans. Aerosp. Electron. Syst.*, vol. 26, no. 2, pp. 337–344, Mar. 1990.



**Woei-Luen Chen** (S'03–M'04) was born in Taiwan, R.O.C., on November 29, 1971. He received the M.S.E.E. degree from the National Taiwan University in 1997. Currently he is a Ph.D. candidate at the Department of Electrical Engineering, NTU.

His current research interests include power electronic applications, reactive power compensation systems, and the wind-energy conversion systems.

**Yuan-Yih Hsu** (S'82–M'82–SM'89) was born in Taiwan, R.O.C., on June 19, 1955. His current research interests include power system dynamics and stability analysis, distribution automation, and the application of artificial intelligence to power systems.

Since 1977, he has been with the National Taiwan University, where he is now a Professor.